JOURNAL OF GEOPHYSICAL RESEARCH, VOL. 113, A10105, doi:10.1029/2008JA013030, 2008

Comment on "Prediction of the 1-AU arrival times of CME-associated interplanetary shocks: Evaluation of an empirical interplanetary shock propagation model" by K.-H. Kim et al.

N. Gopalswamy[1] and H. Xie[2]

Received 9 January 2008; revised 11 June 2008; accepted 28 July 2008; published 23 October 2008.

Citation: Gopalswamy, N., and H. Xie (2008), Comment on ''Prediction of the 1-AU arrival times of CME-associated interplanetary shocks: Evaluation of an empirical interplanetary shock propagation model'' by K.-H. Kim et al., *J. Geophys. Res.*, *113*, A10105, doi:10.1029/2008JA013030.

[1] Recently, *Kim et al.* [2007] (hereinafter referred to as KMC) have evaluated the empirical shock arrival (ESA) model and found only about 60% of the observed shocks arrived within ±12 h of the model prediction. They also found the deviations of shock travel times from the ESA model strongly correlate with the CME initial speeds (V_{CME}), suggesting that the constant interplanetary (IP) acceleration used in the ESA model may not be applicable to all CMEs. KMC further concluded that faster CMEs decelerate and slower CMEs accelerate more than that what is considered in the ESA model. In other words, the average speeds of slower CMEs must be higher than predicted, while those of the faster CMEs must be smaller than predicted. Even though they recognized that *Kim et al.* [2007, paragraph 22] "do not exclude the possibility that the projection effect would be the main cause of the deviations from the ESA model," they did not include it in their comparison with the ESA model. We point out that such systematic deviations in arrival time arise owing to projection effects.

[2] The key ingredient of the ESA model and the parent empirical CME arrival (ECA) model is the IP acceleration profile of the CMEs. The acceleration profile was first derived empirically by *Gopalswamy et al.* [2000] using CME observations from the Solar and Heliospheric Observatory (SOHO) and Wind observations of the corresponding IP CMEs (ICMEs). The ESA model is a simple extension of the ECA model, in that the arrival of shocks preceded the CME arrival by an interval given by the shock standoff distance [*Gopalswamy et al.*, 2005a, 2005b]. Since SOHO provides CME information in the sky plane, the measured speeds are subject to projection effects, so *Gopalswamy et al.* [2001] obtained a new acceleration profile using data from Helios and P78–1 missions [*Sheeley et al.*, 1985; *Lindsay et al.*, 1999] when the spacecraft were in quadrature (so the projection effects were minimal).

[3] Thus, the acceleration profile used by the ESA model requires that the CME initial speed be devoid of projection effects. The projection effects are severe for CMEs originating close to the disk center, many of which are expected to be halo CMEs. *Xie et al.* [2006] has already shown that when the deprojected CME speed obtained using a cone model is used as input to the ESA model, the prediction is substantially improved. For CMEs originating close to the disk center, the space speed is expected to be higher than the sky-plane speed, so the arrival times will be smaller and get closer the model curve. In fact, the ESA and ECA models require that CMEs originate close to the disk center of the Sun. This requirement has been stated by *Gopalswamy et al.* [2005a] as follows: ''we have assumed that what we observe at 1 AU is the nose of the magnetic cloud and shock. This is mostly true for magnetic clouds, but appropriate modifications have to be made when the CMEs are ejected off of the Sun–Earth line.'' The appropriate modification is to consider the Earth-directed speed of the CME, rather than the sky-plane speed of the CME. It is known that CMEs associated with magnetic clouds originate close to the central meridian, while those associated with noncloud ICMEs generally originate at large angles to the Sun-Earth line [*Gopalswamy*, 2006; *Gopalswamy et al.*, 2008]. In fact, KMC used data from *Manoharan et al.* [2004], who considered only CMEs with solar sources located within ±30° from the Sun center (the central zone). Since the Earthward component is expected to be smaller than the sky-plane speed for CMEs at larger angles to the Sun-Earth line (i.e., outside the central zone), the Sun-Earth travel time will shift to larger values when the correction is applied. The combined effect of the two projection corrections (using space speed and Earthward speed) is that the low-speed outliers move to the right and the high-speed ones move to the left producing better agreement with the ESA model.

[4] In order to correct for the projection effects, we need to use a cone model. Several CME cone models exist in the literature (see *Xie et al.* [2006] for details), but here we consider a simple model to illustrate the importance of projection effects. The ultimate aim is to compute the Earthward speed (V_E) from the sky-plane speed (V_S). To do this, we need to input the heliographic coordinates of the

[1]NASA Goddard Space Flight Center, Greenbelt, Maryland, USA.
[2]Department of Physics, Catholic University of America, Washington, D.C., USA.

0148-0227/08/2008JA013030$09.00

CME source location and the angular half width (W) of the CME along with V_S into the cone model to get the CME space speed as the output. We then project the space speed along the Sun-Earth line to get V_E. The only parameter difficult to obtain is the CME width, which is unknown for halo CMEs and for wide CMEs occurring on the disc. We consider a set of 341 CMEs which originated within 30° from the limb as determined from the locations of the associated flares (see *Yashiro et al.* [2008] for details). Since measurements of these CMEs are not subject to significant projection effects, we assign an average half width (W) to each speed range and take it as the cone half angle: 66° ($V_S \geq 900$ km/s), 45° (500 km/s < V_S < 900 km/s), and 32° ($V_S \leq 500$ km/s). The three speed ranges roughly correspond to the low-speed, medium-speed, and high-speed CMEs in the list of CMEs used for testing the ESA model (see below).

[5] Table 1 lists the CMEs used by KMC along with their candidate solar source locations. CME date, time, V_S, V_E, heliographic coordinates of solar sources, deviation (ΔT_S) of the observed shock travel time (T_{sh}) from the ESA model when V_S is used, deviation (ΔT_E) when V_E is used, and an event group index (1 to 3) are listed in Table 1. CMEs are divided into three groups depending on the value of ΔT_S: (1) 13 events (events 53 to 65 in Table 1) with $\Delta T_S < -12$ h (observed travel time is larger than the ESA model prediction by more than 12 h), (2) 52 events (events 1 to 52 in Table 1) with ΔT_S within ±12 h, and (3) 16 events (events 66–81) with $\Delta T_S > 12$ h. These groups can be regarded as low-speed (average ~507 km/s), medium-speed (average ~816 km/s), and high-speed (average ~1289 km/s) groups, with their half widths given above.

[6] Note that we have used only 81 of the 91 events listed by KMC because we think the source locations for 9 events (19 November 1997, 26 December 1997, 28 February 1998, 29 June 1999, 1 August 1999, 20 June 2000, 15 June 2001, 20 March 2002, and 29 July 2002) are backsided or behind the limb, so the CME-shocks pairs are likely to be incorrect for these cases. For one event (7 March 1999), the solar source is correct, but the CME could not be measured, so we exclude it from the study. The number of shocks with their travel times deviating by > 12 h from the ESA model curve ($|\Delta T_S| > 12$ h) is thus slightly different (29 out of 81 events versus 36 out of 91 events). We have also updated the source locations and speeds of a few CMEs.

[7] Once projection corrections are applied, the shock travel times change in all the groups. Table 2 summarizes the changes in the number of events outside the ±12 h window and the mean deviation from the ESA model for each CME group. The averages of V_E and V_S have the following relation: $V_E > V_S$ for group 2 (690 versus 507 km/s), V_E and V_S are about the same in group 1 (762 versus 816 km/s), and $V_E < V_S$ for group 3 (1029 versus 1289 km/s). Projection corrections take T_{sh} outside the ±12 h window in 9 cases ($|\Delta T_E| > 12$ h) in group 2. In group 1, in all but 3 cases T_{sh} moves inside the ±12 h window. In group 3, T_{sh} moves inside the ±12 h window in 8 cases, but the deviations decrease for all but one event. The single exception is event 69 (18 January 2000) for which the deviation increased from 13 h to 23 h. The net result is that $|\Delta T_E| > 12$ h only in 20 cases (compared to the 29 before correction). Thus, the travel times of 61 of the

Table 1. List of Events With Solar Sources Used for Testing the ESA Model

Event	CME Date	Time	V_S[a]	V_E[b]	Location[c]	ΔT_S[d]	ΔT_E[e]	Group[f]
1	6 Jan 1997	1510	136	194	S18E06	−10	−9	2
2	21 May 1997	2100	296	472	N05W12	0	6	2
3	30 Aug 1997	0130	371	349	N30E17	7	6	2
4	6 Oct 1997	1528	293	130	S54E46	8	4	2
5	4 Nov 1997	0610	785	744	S14W33	3	0	2
6	6 Dec 1997	1027	397	232	N49W12	4	0	2
7	2 Jan 1998	2328	438	274	N24W42	2	−3	2
8	25 Jan 1998	1526	693	696	N21E25	4	4	2
9	15 Oct 1998	1004	262	354	N22W01	−9	−6	2
10	4 Nov 1998	0754	523	657	N17W01	−8	0	2
11	13 Apr 1999	0330	291	439	N16E00	−10	−5	2
12	24 Jun 1999	1331	975	814	N29W13	5	−6	2
13	28 Jul 1999	0906	462	707	S15E03	−2	13	2
14	25 Oct 1999	1426	511	441	S38W15	−12	−15	2
15	10 Feb 2000	0230	944	791	N31E04	−6	−16	2
16	12 Feb 2000	0431	1107	899	N26W23	8	−3	2
17	17 Feb 2000	2006	728	762	S29E07	7	9	2
18	4 Apr 2000	1632	1188	915	N16W66	9	−5	2
19	6 Jun 2000	1554	1119	991	N20E15	−1	−7	2
20	10 Jun 2000	1708	1108	799	N22W38	11	−8	2
21	11 Jul 2000	1327	1078	900	N17E27	0	−10	2
22	14 Jul 2000	1054	1674	1501	N22W07	2	−1	2
23	25 Jul 2000	0330	528	721	N06W08	−5	8	2
24	4 Sep 2000	0606	849	742	N13W38	1	−7	2
25	2 Oct 2000	0350	525	706	S09E07	−9	3	2
26	9 Oct 2000	2350	798	1040	N01W14	9	25	2
27	25 Oct 2000	0826	770	418	N17W70	10	−12	2
28	1 Nov 2000	1626	801	670	S17E39	−3	−13	2
29	8 Nov 2000	2306	1738	1256	N10W75	7	−5	2
30	16 Mar 2001	0350	271	423	N11W09	−11	−6	2
31	19 Mar 2001	0526	360	661	S05W00	−8	8	2
32	24 Mar 2001	2050	906	792	N15E22	−1	−9	2
33	6 Apr 2001	1930	1270	999	S21E31	4	−8	2
34	9 Apr 2001	1554	1192	1081	S21W04	7	2	2
35	11 Apr 2001	1331	1103	895	S22W27	−1	−12	2
36	26 Apr 2001	1230	1006	916	N20W05	−7	−12	2
37	9 Aug 2001	1030	479	849	N05W05	−10	15	2
38	14 Aug 2001	1601	618	550	N16W36	−8	−12	2
39	11 Sep 2001	1454	791	729	N13E35	−3	−8	2
40	28 Sep 2001	0854	846	1015	N10E18	1	11	2
41	9 Oct 2001	1130	973	832	S28E08	4	−5	2
42	19 Oct 2001	1650	901	746	N15W29	−6	−17	2
43	4 Nov 2001	1635	1810	1664	N06W18	10	8	2
44	22 Nov 2001	2330	1437	1095	S17W36	0	−12	2
45	14 Feb 2002	0230	473	321	S43W11	−11	−16	2
46	15 Mar 2002	2306	957	913	S08W03	12	9	2
47	15 Apr 2002	0350	720	960	S15W01	−12	5	2
48	17 Apr 2002	0826	1240	981	S14W34	12	0	2
49	7 May 2002	0406	720	767	S10E27	12	15	2
50	8 May 2002	1350	614	802	S12W07	−7	7	2
51	15 Jul 2002	2130	1300	1194	N19W01	7	4	2
52	24 Nov 2002	2030	1077	817	N20E35	5	−11	2
53	7 Feb 1997	0030	490	728	S20W04	−21	−6	1
54	12 May 1997	0530	464	673	N21W08	−15	−2	1
55	3 Jul 1999	1954	536	567	N18W55	−13	−11	1
56	13 Sep 1999	1731	444	696	N15E06	−34	−18	1
57	20 Sep 1999	0606	604	773	S20W05	−21	−9	1
58	7 Jul 2000	1026	453	679	N17E10	−16	−2	1
59	9 Aug 2000	1630	702	882	N20E12	−18	−5	1
60	3 Nov 2000	1826	291	556	N02W02	−26	−15	1
61	28 Feb 2001	1450	313	518	S02W12	−20	−12	1
62	25 Mar 2001	1706	677	817	N16E25	−22	−11	1
63	19 Apr 2001	1230	392	534	N20W20	−35	−29	1[g]
64	27 Sep 2001	0806	669	790	S20W27	−21	−12	1
65	29 Jul 2002	1207	562	754	S10W10	−13	0	1
66	29 Apr 1998	1659	1374	1200	S18E20	20	14	3
67	5 Nov 1998	2044	1118	964	N22W18	14	6	3
68	12 Sep 1999	0054	732	613	S17W39	13	4	3
69	18 Jan 2000	1754	739	870	S19E11	13	23	3
70	8 Feb 2000	0930	1079	864	N25E26	21	9	3
71	12 Sep 2000	1154	1550	1404	S12W18	36	33	3[h]
72	20 Jan 2001	2130	1507	1028	S07E46	32	15	3

Table 1. (continued)

Event	CME Date	Time	V_S[a]	V_E[b]	Location[c]	ΔT_S[d]	ΔT_E[e]	Group[f]
73	5 Apr 2001	1706	1390	811	S24E50	16	−12	3
74	15 Apr 2001	1406	1199	832	S20W85	20	0	3
75	25 Aug 2001	1650	1433	1118	S17E34	20	9	3
76	22 Oct 2001	1506	1336	1160	S21E18	32	25	3
77	25 Oct 2001	1526	1092	957	S16W21	17	9	3
78	17 Nov 2001	0530	1379	986	S13E42	28	12	3
79	26 Dec 2001	0530	1446	836	N08W54	41	13	3
80	16 Aug 2002	1230	1585	1410	S14E20	27	22	3
81	5 Sep 2002	1654	1657	1414	N09E28	22	16	3

[a]Sky-plane speed in km/s.
[b]Earthward speed in km/s.
[c]Heliographic coordinates of CME sources.
[d]Deviation (hours) of the shock travel time from the ESA model when sky-plane speed is used.
[e]Deviation (hours) of the shock travel time from the ESA model when deprojected speed is used.
[f]Group 1, low-speed events with $\Delta T_S < -12$ h; group 2, medium-speed events with ΔT_S within ±12 h; and group 3, high-speed events with $\Delta T_S >$ 12 h.
[g]A low-speed outlier discussed in the text.
[h]A high-speed outlier discussed in the text.

81 shocks (or 75.3%) agree with the ESA model when projection effects are taken into account. Furthermore, the average deviations also decrease significantly for both the low-speed (from 21.2 h to 10.2 h) and high-speed (from 23.2 h to 13.9 h) groups. For the intermediate-speed group 2, the change is relatively small (increases from 6.3 h to 8.2 h). The overall average deviation (all the groups combined) decreases from 12.1 h ($|\Delta T_S|$) to 9.6 h ($|\Delta T_E|$).

[8] Table 2 shows that most of the events in group 1 are within the central zone except for event 55 and $|\Delta T_E|$ becomes $\leq$ 12h after projection correction. Event 55 is from N18W55, which moves from marginally outside to marginally inside the ±12 h window. In group 3, there are 7 events outside the central zone (9 inside). After projection correction, 5 of the 7 moved inside the ±12 h window, while the remaining two are only slightly outside the ±12 h window. For group 2, there are 18 events outside the central zone. Projection corrections resulted in only four of these events moving outside the ±12 h window. Five other events that moved outside the ±12 h window are from inside the central zone.

[9] Figure 1 compares the shock travel times (T_{sh}) obtained using V_S and V_E as input to the ESA model. Figure 1a is similar to the plot of KMC, except for the reduced number of events as described above. We see that (1) almost all the low-speed outliers have moved to the right (closer to the model curve) when projection correction is applied, (2) most of the high-speed outliers move to the left (again closer to the model curve), (3) some data points originally within the ±12 h window have moved outside because of the projection corrections, and (4) there are still some high-speed events with T_{sh} outside the ±12 h window.

[10] There is a single outlier in Figure 1b on the low-speed side corresponding to the shock on 21 April 2001 (event 62 in Table 1). The shock was identified with the CME on 19 April 2001. We are confident that there is no competing candidate CME. The CME originated from the northwest quadrant (N32W23) and moves mostly above the northwest limb with $V_S \sim$ 392 km/s and $V_E \sim$534 km/s. The observed travel time for the shock is ∼50 h. With V_S = 392 km/s, the ESA model yields $T_{sh} \sim$85 h. With V_E = 534 km/s, the ESA model yields $T_{sh} \sim$79 h. Thus the improvement due to projection correction is marginal for this case and the deviation remains substantial (∼29 h). When we examined the SOHO EUV images, we found a coronal hole located immediately to the east of the CME-producing active region. The fast wind from the coronal hole is likely to have kept the CME from decelerating, resulting in a shorter travel time. The outlier on the high-speed side corresponds to the 12 September 2000 event, associated with an extended filament eruption centered on S12W18. The CME was one of the fastest (V_S = 1550 km/s), yet it took ∼64 h for the shock to arrive at L1. When we examined the EUV images, we found that there was an extended coronal hole parallel to the preeruption filament, located between the disk center and the CME source (filament). The coronal hole might have confined the CME to the south, thus allowing only the weak flank of the CME arrive at Earth. Thus the V_E is expected to be smaller than the one obtained using the cone model. A speed smaller than the V_E listed in Table 1, would explain the large T_{sh}. These two events demonstrate that conditions in the ambient medium (ahead and behind the CME) may also affect the shock travel time. It may be necessary to look into the source regions of the other outliers in Figure 1b to understand the remaining deviations, but this is beyond the scope of this report.

[11] The 75% success rate obtained after projection correction is substantial, given the simplicity of the ESA model (uses a single input parameter, namely, the CME speed near the Sun). Note that this rate is roughly the same as the result from KMC's linear regression analysis, which gives a shock transit time (in hours) $T = 76.86 - 0.02V_{CME}$ (such a relation was also obtained by *Gopalswamy et al.* [2005a]: $T = 84.25 - 0.03V_{CME}$, which was based on data free from projection effect). For a 2000 km/s CME, *Gopalswamy et al.*'s [2005a] regression line gives an arrival time of 24.25 h,

Table 2. Summary of Changes Due to Projection Correction

Group	Number of Events	Number of ΔT_S > 12 h	Number of ΔT_E > 12 h	Number of Central	$\langle V_S \rangle$ (km/s)	$\langle V_E \rangle$ (km/s)	$\langle \Delta T_S \rangle$ (h)	$\langle \Delta T_E \rangle$ (h)
1	13	13	3	12	507	690	21.2	10.2
2	52	0	9	34	816	762	6.3	8.2
3	16	16	8	9	1289	1029	23.2	13.9
All	81	29	20	55	860	803	12.1	9.6

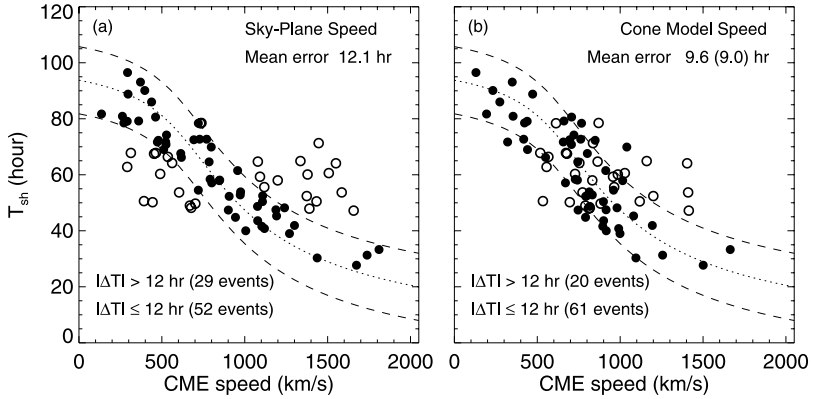

Figure 1. Travel times for 81 shocks plotted as a function of the CME initial speed (a) for sky-plane speeds and (b) for Earthward speeds. The ESA model curve is shown as the dotted line. The two dashed curves on either side of the ESA model curve correspond to ±12 h deviations. The solid circles in Figure 1a represent shocks agreeing with the ESA model within ±12 h, while the open circles represent those outside this band. In Figure 1b, we have not changed the symbols, so that the solid and open circles were redistributed owing to projection correction. Note that many open circles moved into the ±12 h band, while some solid circles moved outside. The mean error drops from 12.1 h to 9.6 h after the projection corrections (the error is 9.0 h when the two outliers are excluded).

while KMC gives ∼50% higher value (36.86 h) mainly because of the bias at high speeds caused by projection effects. One of the main problems with the regression lines is that they do not apply to the highest-speed events. Since the ESA model was derived independently (without the data points in KMC) and applies to higher-speed CMEs, it has a better prediction value.

[12] KMC also pointed out that CME mass may play an important role because it figures in the drag coefficient. The ESA model is kinematic and does not include mass explicitly. However, it is worth studying if the travel time depends on CME mass. It must be noted that the mass measurements are not very accurate [*Vourlidas et al.*, 2000] especially for disk events. While the major deviations in travel time can be explained by taking proper account of the projection effects, there is still some scattering in the travel time versus CME speed plot in Figure 1b. We think the main source of scattering is likely from the empirical model used for the acceleration (a, m s^{-2}) profile: $a = -0.0054\ (V_{CME} - 406.11)$, where the initial speed of CMEs (V_{CME}) is in km/s. This profile assumes that the average solar wind speed is ∼406 km/s. But the solar wind speed can easily be different from ∼406 km/s. Uncertainties are thus expected in the acceleration profile when the ambient solar wind speed is substantially different from the above value. One such case was already discussed (19 April 2001 event). Additional factors include: (1) the acceleration cessation distance used by *Gopalswamy et al.* [2001] may not apply for very fast CMEs that continue to decelerate beyond 1 AU. This may be the case for the events with large deviations at high speeds in Figure 1b. (2) Possible misidentification of CMEs associated with some ICMEs. If the CME is misidentified, the shock travel time can be substantially different and hence contributes to the scattering. (3) Some solar sources are extended, so there may be uncertainty in the heliographic coordinates used as cone model input.

[13] In summary, the simple ESA model predicts the arrival time of shocks within ±12 h in ∼75% of cases when projection effects are taken into account; the average error in the travel time of the remaining events is also significantly reduced. We do appreciate that the ESA model is a single-parameter model, so deviations are expected, especially when CMEs propagate into different environments.

[14] **Acknowledgments.** Work supported by NASA's LWS TR&T program.

[15] Amitava Bhattacharjee thanks the reviewer for their assistance in evaluating this paper.

References

Gopalswamy, N. (2006), Properties of interplanetary coronal mass ejections, *Space Sci. Rev.*, *124*, 145, doi:10.1007/s11214-006-9102-1.

Gopalswamy, N., A. Lara, R. P. Lepping, M. L. Kaiser, D. Berdichevsky, and O. C. St. Cyr (2000), Interplanetary acceleration of coronal mass ejections, *Geophys. Res. Lett.*, *27*, 145, doi:10.1029/1999GL003639.

Gopalswamy, N., A. Lara, S. Yashiro, M. L. Kaiser, and R. A. Howard (2001), Predicting the 1-AU arrival times of coronal mass ejections, *J. Geophys. Res.*, *106*, 29,207, doi:10.1029/2001JA000177.

Gopalswamy, N., A. Lara, P. K. Manoharan, and R. A. Howard (2005a), An empirical model to predict the 1-AU arrival of interplanetary shocks, *Adv. Space Res.*, *36*, 2289, doi:10.1016/j.asr.2004.07.014.

Gopalswamy, N., S. Yashiro, Y. Liu, G. Michalek, A. Vourlidas, M. L. Kaiser, and R. A. Howard (2005b), Coronal mass ejections and other extreme characteristics of the 2003 October–November solar eruptions, *J. Geophys. Res.*, *110*, A09S15, doi:10.1029/2004JA010958.

Gopalswamy, N., S. Akiyama, S. Yashiro, G. Michalek, and R. P. Lepping (2008), Solar sources and geospace consequences of interplanetary magnetic clouds observed during solar cycle 23, *J. Atmos. Sol. Terr. Phys.*, *70*, 245, doi:10.1016/j.jastp.2007.08.070.

Kim, K.-H., Y.-J. Moon, and K.-S. Cho (2007), Prediction of the 1-AU arrival times of CME-associated interplanetary shocks: Evaluation of an empirical interplanetary shock propagation model, *J. Geophys. Res.*, *112*, A05104, doi:10.1029/2006JA011904.

Lindsay, G. M., J. G. Luhmann, C. T. Russell, and J. T. Gosling (1999), Relationships between coronal mass ejection speeds from coronagraph images and interplanetary characteristics of associated interplanetary coronal mass ejections, *J. Geophys. Res.*, *104*, 12,515.

Manoharan, P. K., N. Gopalswamy, S. Yashiro, A. Lara, G. Michalek, and R. A. Howard (2004), Influence of coronal mass ejection on propagation of interplanetary shocks, *J. Geophys. Res.*, *109*, A06109, doi:10.1029/2003JA010300.

Sheeley, N. R., R. A. Howard Jr., D. J. Michels, M. J. Koomen, R. Schwenn, K. Muehlhaeuser, and H. Rosenbauer (1985), Coronal mass ejections and interplanetary shocks, *J. Geophys. Res.*, *90*, 163.

Vourlidas, A., P. Subramanian, K. P. Dere, and R. A. Howard (2000), Large angle spectrometric coronagraph measurements of the energetics of coronal mass ejections, *Astrophys. J.*, *534*, 456, doi:10.1086/308747.

Xie, H., N. Gopalswamy, L. Ofman, O. C. St. Cyr, G. Michalek, A. Lara, and S. Yashiro (2006), Improved input to the empirical coronal mass ejection (CME) driven shock arrival model from CME cone models, *Space Weather*, *4*, S10002, doi:10.1029/2006SW000227.

Yashiro, S., G. Michalek, S. Akiyama, N. Gopalswamy, and R. A. Howard (2008), Spatial relationship between solar flares and coronal mass ejections, *Astrophys. J.*, *673*, 1174, doi:10.1086/524927.

N. Gopalswamy, NASA Goddard Space Flight Center, Building 21, Room 260, Code 695, Greenbelt, MD 20771, USA. (gopals@ssedmail.gsfc.nasa.gov)

H. Xie, Department of Physics, Catholic University of America, 200 Hannan Hall, Washington, DC 20064, USA.